Original article

The influence of heterogeneous structure on salt precipitation during CO_2 geological storage

Di He[1], Peixue Jiang[2], Ruina Xu[2]*

[1]*Fujian Province Green and Intelligent Manufacturing Technology Economic Integration Service Platform, Fujian Key Laboratory of Green Intelligent Cleaning Technology and Equipment, School of Mechanical and Automotive Engineering, Xiamen University of Technology, Xiamen 361024, P. R. China*

[2]*Key Laboratory for CO_2 Utilization and Reduction Technology of Beijing, Department of Energy and Power Engineering, Tsinghua University, Beijing 100084, P. R. China*

Abstract:
The presence of rock heterogeneity and fractures may cause abrupt spatial changes in capillary action and flow characteristics, which eventually change the precipitation behavior during CO_2 geological storage. Therefore, the salt precipitation mechanism of the heterogeneous structure needs to be studied. In this paper, the salt precipitation behavior in different heterogeneous structures was studied through pore-scale experiments at room temperature and atmospheric conditions. In the up-down heterogeneous structure, the salt precipitation has little effect on the injectivity regardless of the CO_2 injection rate. When the CO_2 injection rate is low, the salt tends to precipitate in situ in the small pore structure to form a crystal structure. When the CO_2 injection rate is high, the salt tends to precipitate in the large pore structure to form a cluster structure. In the left-right heterogeneous structure, regardless of the CO_2 injection rate, the precipitated salt is mainly in the cluster structure, and the salt is more dispersed in distribution, the impact on injectivity is small. The injection well can be selected in the formation with strong heterogeneity, to alleviate the blockage caused by salt precipitation. When CO_2 leaks in the fractures, salt tends to grow until the fracture is plugged, which is of great significance for the self-healing of the fracture for the caprock.

1. Introduction

CO_2 geological storage is an effective way to deal with global climate change (Bentham and Kirby, 2005; Yang et al., 2014; Liu et al., 2020; Ren et al., 2021). The saline aquifer is an ideal reservoir for CO_2 geological storage due to the advantage of large storage capacity (Yang et al., 2014; Salih et al., 2017). The injectivity of CO_2 is an essential indicator in CO_2 geological storage. The decrease in injectivity caused by salt precipitation is more serious near the injection well (Bacci, 2011; Grude et al., 2014; Piao et al., 2018; Akindipe et al., 2021; Norouzi et al., 2022). CO_2 geological storage projects such as Ketzin (Baumann et al., 2014) and Snøhvit (Grude et al., 2014) have found the problem of poor injectivity caused by salt precipitation. Due to the continuous

injection of a large amount of dry CO_2, the water in the brine is continuously evaporated into the CO_2 phase and carried away. The concentration of the brine gradually increases and eventually reaches supersaturation. Salt will precipitate in the pores, change the porosity and permeability of the reservoir, and ultimately affect the injectivity of CO_2. In severe cases, a complete blockage may occur (Tang et al., 2015; Cui et al., 2023).

Many laboratory studies and numerical simulations have been carried out on the salt precipitation problem during CO_2 injection. The effects of thermodynamic conditions like temperature, pressure, and salt concentration (Bacci et al., 2013; Nooraiepour et al., 2018), the CO_2 injection rate (Wang et al., 2009, 2010; Ott et al., 2015), and rock properties (Tang et al., 2015; Hu et al., 2022) (porosity and permeability) on
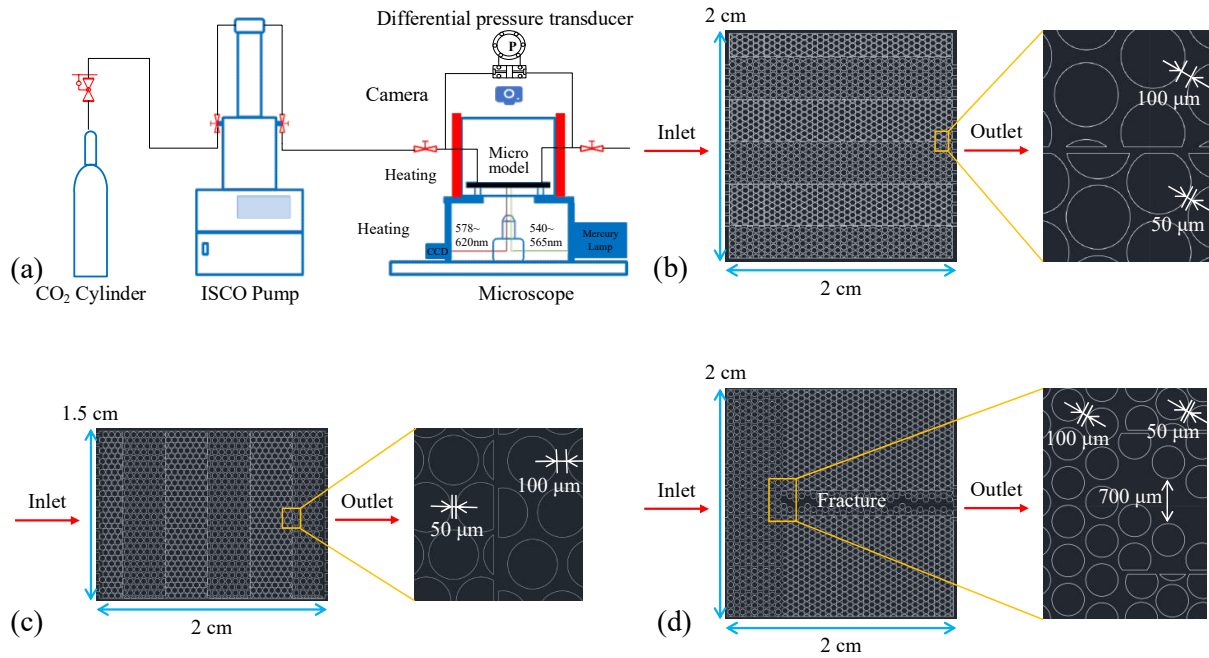
Fig. 1. Experimental system and micromodel structure diagram: (a) experimental system, (b) up-down heterogeneous micromodel, (c) left-right heterogeneous micromodel and (d) composite micromodel.

salt precipitation behavior were studied. For the vicinity of reservoir injection wells, it is necessary to reduce or even avoid salt precipitation to alleviate the effect of salt precipitation on injection. He et al. (2019) studied the mechanism of salt precipitation in homogeneous porous media and its influence on permeability. It was found that under hydrophilic conditions when the CO_2 injection rate was small, salt accumulated in the injection front and mainstream area, seriously damaging the reservoir's injectivity. While increasing the parameters such as CO_2 injection rate and contact angle could reduce the effect of salt precipitation on injectivity. In actual formations, the rock structure is very complex, and the rock may contain various types of mineral layers, textures, and interfaces between mineral layers formed by natural evolutionary processes such as mineral deposition and erosion (Bergstad et al., 2018). The long-term safety of CO_2 geological storage is an important index to evaluate the target reservoir, which requires the target reservoir to have long-term caprock integrity. However, in actual projects, the injection of CO_2 may cause overpressure in the caprock, and the reservoir pressure exceeds the capillary breakthrough pressure of the caprock, resulting in CO_2 leakage. The injection of CO_2 may also lead to the activation of old fractures in the caprock or even overpressure to form new fractures. In addition, there may be existing fracture systems that are not detected below the resolution of seismic data. These would be potential pathways for CO_2 leakage through caprocks (Vialle et al., 2016). For caprocks, if salt precipitation can plug the fractures, will achieve the effect of fracture self-healing (He et al., 2022). The existence of rock heterogeneity and fractures may cause abrupt spatial changes in capillary action (Cai et al., 2014, 2022) and flow characteristics, and change the process of fluid transport, which may eventually

change the precipitation behavior and spatial distribution of salt. Therefore, the salt precipitation mechanism and law of heterogeneous structure need to be further studied.

Therefore, this paper will carry out pore-scale experiments to study the effect of different CO_2 injection rates on the precipitation behavior of salt in fractures and heterogeneous structures, and explore the mechanism of salt precipitation in heterogeneous structures and the self-healing mechanism of salt precipitation in fractures.

2. Experimental system and method

2.1 Experimental system and micromodel

As shown in Fig. 1(a), the experimental device was similar to the previous experimental platform of our research group (Li et al., 2017; Xu et al., 2017; He et al., 2019). The CO_2 cylinder with a pressure-reducing valve (CO_2 purity of 99.99%) is connected to a high-pressure plunger pump (Teledyne ISCO, 500D) to ensure accurate adjustment of the CO_2 flow injected into the micromodel. Differential pressure is measured using a differential pressure transducer (EJA430E). During the experiment, to obtain a full field of view and fast imaging, a Canon EOS-7D camera equipped with a MACRO 100 mm lens automatically takes photos every few seconds. After the experiment, a Nikon Ti-E inverted microscope (resolution of 1.83 μm under 5 objective lenses) was used to observe the salt precipitation microstructure in the micromodel. The micromodel is made of silica substrate etched with hydrofluoric acid (Kim et al., 2013), the wettability is hydrophilic and the contact angle is approximately 22°.

Figs. 1(b)-1(d) are the structure of the three different micromodels, in which Fig. 1(b) is an up-down heterogeneous

Table 1. List of experimental conditions.

Type	Case	CO_2 injection rate (mL/min)	Capillary number (-)	Total time (h)
Up-down	UD-1	0.1	2.79×10^{-6}	63.7
	UD-2	0.5	1.40×10^{-5}	12.5
	UD-3	2	5.59×10^{-5}	3.0
Left-right	LR-1	0.1	3.49×10^{-6}	9.1
	LR-2	0.5	1.75×10^{-5}	7.4
	LR-3	2	6.99×10^{-5}	2.5
Composite microstructure	CO-1	0.1	2.00×10^{-6}	143
	CO-2	2	3.99×10^{-5}	8

micromodel. From top to bottom, the porous regions of the large aperture and small aperture are distributed in turn, in which the pore throat of the large aperture is 100 μm and the pore throat of the small aperture is 50 μm. The pore volume is approximately 5.9 μL. Fig. 1(c) is a left-right heterogeneous micromodel, and the porous regions with large and small apertures are distributed from left to right, in which the pore throat with a large aperture is 100 μm and the pore throat with a small aperture is 50 μm. The pore volume is approximately 4.6 μL. Fig. 1(d) is a composite micromodel, including fractures, large-aperture porous regions, and small-aperture porous regions. The area near the inlet is a large aperture porous area with a pore throat of 100 μm, and the right side is a small aperture porous area with a pore throat of 50 μm. A fracture with a width of 700 μm is opened in the middle of the small aperture porous area. The pore volume is approximately 3.5 μL. The etching depth of the three micromodels is 45 μm.

2.2 Experimental procedure and conditions

The sodium chloride solution with a mass fraction of 20% was prepared with high-purity sodium chloride and deionized water. The air dissolved in the solution was extracted by a vacuum pump. To prevent residual air in the micromodel, the first injection of large amounts of CO_2 to replace the air, and then with at least 100 times the pore volume of sodium chloride solution to displace and dissolve the CO_2 in the micromodel, until the sodium chloride solution fully saturated pore volume of the micromodel. The micromodel saturated with solution is loaded horizontally into the autoclave. In this paper, three CO_2 injection rates (0.1, 0.5 and 2 mL/min) are designed, and the capillary number ranges from 2.00×10^{-6} to 6.99×10^{-5} which can be matched to that in the Quest CCS Project in Canada (around 4.5×10^{-6}) (Duong et al., 2019; He et al., 2019). The experimental temperature is room temperature and the pressure is atmospheric. The specific experimental conditions are shown in Table 1. The camera is set to shoot every few seconds to record the salt precipitation state in the micromodel until the solution is completely evaporated. The salt distribution and morphology of the micromodel after salt precipitation were observed by a high-resolution microscope.

3. Results and discussion

3.1 Up-down heterogeneous micromodel

Fig. 2 is the salt precipitation process (UD-1) of the up-down heterogeneous micromodel at a CO_2 injection rate of 0.1 mL/min. In the beginning, the whole micromodel was filled with salt solution (as shown in Fig. 2(a)). CO_2 was injected from the left inlet, and the solution in the porous medium began to be replaced after 1.7 h. It can be seen from Fig. 2(b) that CO_2 preferentially displaced the solution in the large pore area because the larger the pore size, the smaller the capillary resistance. When CO_2 completely breaks through the porous region, the residual solution distribution is shown in Figs. 2(c) and 2(d). It can be seen from the figures that most of the residual solution is distributed in the small pore size porous region. As the CO_2 is continuously injected, the residual solution evaporates (as shown in Figs. 2(e)-2(i)) and the area it occupies gradually decreases. After about 64 h, the solution completely evaporated, and the precipitation of white salt was almost not observed. Instead, as shown in Fig. 2(i), a patch of the same color as the residual solution is seen in the small-pore region, which is further observed by a high-resolution microscope to be transparent crystal structure salt.

Fig. 3(d) shows the salt precipitation structure observed under the microscope after the complete evaporation of the solution. It can be seen from the figure that the precipitated salts are almost colorless and transparent large crystal structures, and ultimately occupy the pore space. From the spatial distribution of salt, it can be seen that salt is mainly distributed in the small pore-size regions (as shown in Fig. 3(a)). Because the residual solution is primarily distributed in the porous region of the small aperture (as shown in Fig. 2(c) and Fig. 2(d)). When the CO_2 injection rate is low, due to the water's low evaporation rate, the salt solute has sufficient time to re-diffuse back into the residual solution under the salt concentration gradient. With the continuous evaporation of water, the salt concentration in the residual solution increases continuously and finally reaches supersaturation. The nucleation rate depends on the concentration. The growth of the critical nucleus in the residual solution will lead to a rapid decrease in local supersaturation and
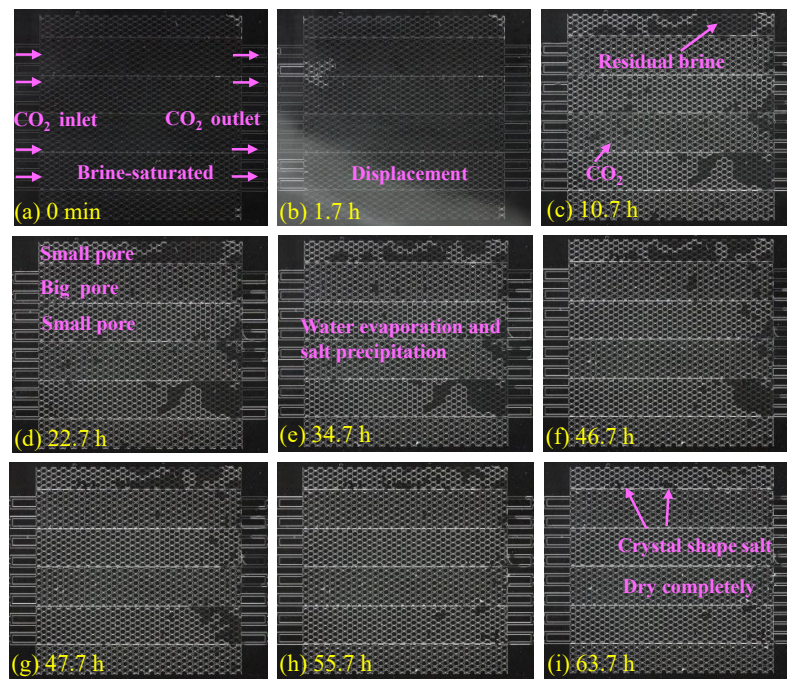
Fig. 2. Salt precipitation process of case UD-1.
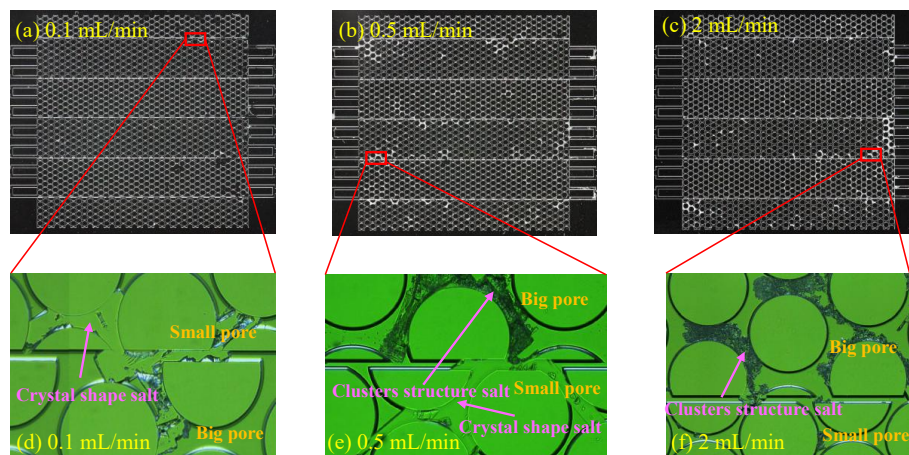
Fig. 3. (a)-(c) The salt distribution under three different CO_2 injection rates in the up-down heterogeneous structures and (d)-(f) microstructure of salt at different injection rates.

a sharp decrease in nucleation rate, which is easy to form crystal shape salt (De Yoreo and Vekilov, 2003). Therefore, when the CO_2 injection rate is low (the evaporation rate is small), the residual solution can easily form isolated crystals of salt structure. Homogeneous nucleation of the salt begins to form inside the residual solution in the small pore size region. As the solution evaporates, the salt gradually grows until the residual solution is completely consumed and the crystal salt stops growing (Kim et al., 2013). At this time, a large crystal structure is formed in the pores of the small pore size porous region. Since the micromodel is an up-down heterogeneous structure, the salt is mainly precipitated in the small pore size porous region, blocking the channels in many small pore size regions. However, there is little salt precipitation in the large

pore-size porous region, which has little effect on the flow of CO_2. From the pressure drop results (as shown in Fig. 5(a)), it can also be seen that after CO_2 completely breaks through the micromodel (about 14 h), the pressure drop begins to decrease. After evaporation is complete, the pressure drop falls to about 1 kPa, so salt precipitation has little effect on the injectivity of CO_2.

Fig. S1 (see the attachment) is the salt precipitation process (UD-2) of the up-down heterogeneous micromodel at a CO_2 injection rate of 0.5 mL/min. After about 5.6 h, CO_2 completely breaks through the porous region, and the residual solution is distributed as shown in Figs. S1(c) and S1(d). It can be seen from the figure that the residual solution is also mainly distributed in the porous region of the small pore
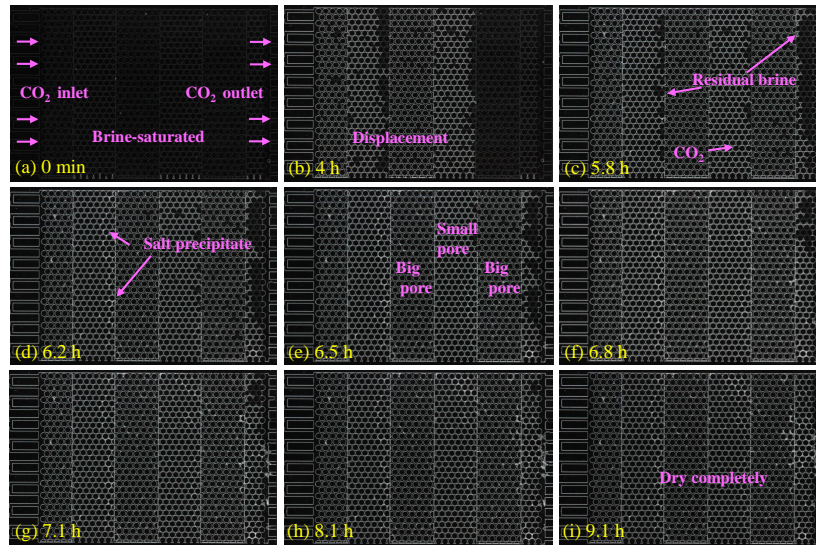
Fig. 4. Salt precipitation process of case LR-1.
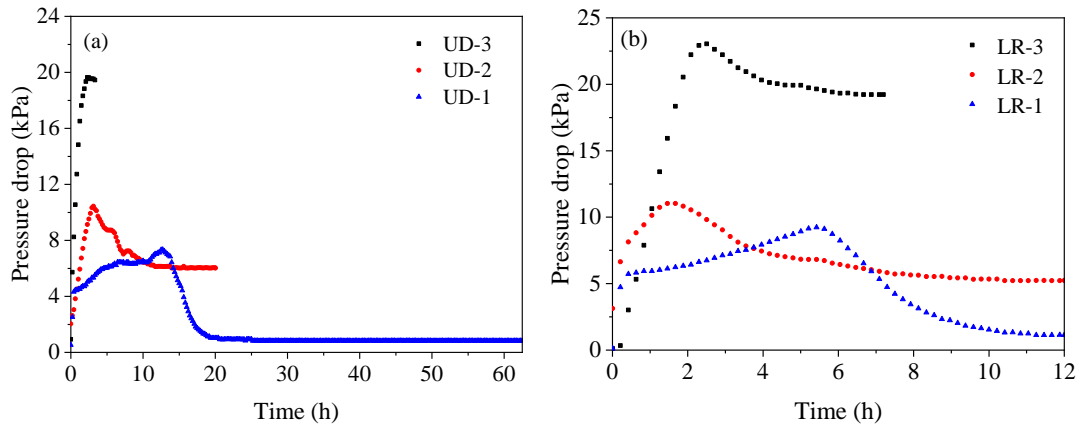
Fig. 5. Pressure drop results under heterogeneous conditions: (a) up-down heterogeneity and (b) left -right heterogeneity.

size, and white salt begins to precipitate at the inlet. With the continuous injection of CO_2 (as shown in Figs. S1(d)-S1(i)), the water evaporates, and the salt precipitates and grows. After 12.5 h (as shown in Fig. S1(i)), the residual solution is wholly consumed. As can be seen from the figure, the color of the precipitated salt is white, which is completely different from that at a low injection rate (colorless or transparent). The microscopic results after salt precipitation are shown in Fig. 3(e). It can be seen from the figure that the precipitated salt has two structures. One is the same large crystal structure as that at a low injection rate (colorless and transparent under the camera). In addition, a cluster structure is added, which is white in Fig. 3(b). From Fig. 3(b), it can be seen that the salt with a cluster structure is mainly distributed in the pores of the large pore size porous region, while the salt with a transparent crystal structure is mainly distributed in the small pore size porous region. This is because as the CO_2 injection rate increases, the water evaporation rate increases, and the solute carried by the reflow liquid film cannot be diffused in time to the residual solution in the small pore size region.

Therefore, the salt with cluster structure tends to be formed at the evaporation front in the large pore-size region. Some salt solutes are homogeneously precipitated in the residual solution in the small pore size region to form crystal salt. The precipitated salt is dispersed in the up-down heterogeneous micromodel, which has little effect on the continuous injection of CO_2. It can also be seen from the pressure drop results (as shown in Fig. 5(a)) that the pressure drop begins to decrease after 3 h and finally maintains at about 6 kPa.

Fig. S2 (see the attachment) is the salt precipitation process (UD-3) of the up-down heterogeneous micromodel at a CO_2 injection rate of 2 mL/min. CO_2 is injected from the left inlet and begins to displace the solution in the porous medium after 10 min. It can be seen from Fig. S2(b) that after the CO_2 injection rate increases, CO_2 still preferentially displaces the solution in the large pore area. It can be seen from the figure that the residual solution state is reached after 50 min of CO_2 injection, and the residual solution is also distributed in the porous area with a small pore size (as shown in Figs. S2(c) and S2(d)). With the continuous injection of CO_2, the
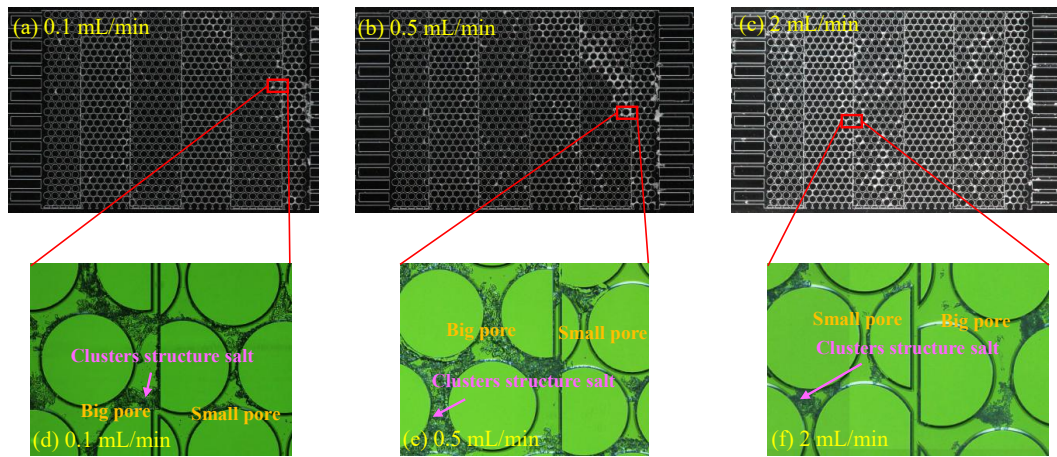
Fig. 6. (a)-(c) Salt distributions at three different CO_2 injection rates in the left-right heterogeneous structure and (d)-(f) microstructure of salt at different injection rates.

salt is continuously precipitated and grown. Finally, after 180 min, the solution is completely evaporated. Compared with the results of the CO_2 injection rate 0.1 mL/min (shown in Fig. 2(i)) and 0.5 mL/min (shown in Fig. S1(i)), it can be found that with the increase of CO_2 injection rate, the time required for evaporation is sharply shortened, indicating that the water evaporation rate increases. It can be seen from Fig. 3(c) that salt is mainly precipitated at the tail of the micromodel. From the microscopic results of salt precipitation in Fig. 3(f), it can be seen that almost all salts are precipitated in a cluster structure. This is because after the injection rate is further increased, the water evaporation rate increases, and the salt solute cannot be diffused into the residual solution in time. Therefore, the salt tends to be ectopically precipitated at the evaporation front in the large pore size region, thereby forming a cluster structure, while the salt is less distributed in the porous region with small pore size. From the pressure drop results in Fig. 5(a), it can be seen that the pressure drop is finally stabilized at about 19 kPa, indicating that the precipitated salt has little effect on the CO_2 injection.

It can be found that regardless of the CO_2 injection rate, salt precipitation has little effect on its permeability in the up-down heterogeneous structures. When the CO_2 injection rate is low, the salt tends to precipitate in situ in the small pore porous region to form a crystal structure. When the CO_2 injection rate increases, the salt tends to precipitate in the large pore structure to form a cluster structure. However, regardless of the structure of salt precipitation, the salt is more dispersed in the micromodel to maintain the flow of the CO_2 channel, so the impact on permeability is small. It should be noted that the experiments were conducted at room temperature, where the temperature is low and the rate of evaporation is low. If the actual formation conditions, the temperature will be higher, thus increasing the evaporation rate of water. It can be predicted that the water evaporation rate will remain high at higher temperatures, even if the CO_2 injection rate is low. Therefore, the salt solute cannot return to the residual solution in the small pores in time and the salt precipitation will tend

to be in the large pores, and precipitate in a cluster structure.

3.2 Left-right heterogeneous micromodel

Fig. 4 shows the salt precipitation process (LR-1) of a left-right heterogeneous micromodel at a CO_2 injection rate of 0.1 mL/min. The micromodel is first filled with salt solution (as shown in Fig. 4(a)), and CO_2 displaced solution in the porous region from the left inlet (as shown in Fig. 4(b)). It can be seen from Fig. 4(c) that CO_2 reaches the residual solution state after 5.8 h of injection, and the residual solution is mainly distributed in the porous region of the small pore size. With the continuous injection of CO_2, the water in the residual solution evaporates, and the salt also precipitates and grows (as shown in Figs. 4(d)-4(i)). Finally, after 9.1 h, the solution completely evaporates. It can be seen from Fig. 4(i) that the salt is mainly precipitated in the small pore porous region of the micromodel. From the microscopic results of salt precipitation in Fig. 6(d), The salt precipitates mainly in cluster form, which is different from the isolated transparent crystal structure formed in the up-down heterogeneous structures (as shown in Fig. 3(d)). This is because, in the left-right heterogeneous structures, CO_2 passes through the porous regions of large and small apertures in turn from left to right, and cannot be selected to pass preferentially in the large aperture porous region. Therefore, even when the CO_2 injection rate is low, CO_2 can fully contact the residual solution in the small aperture porous region to form a forced convection, which fully removes the evaporated water vapor, thereby promoting evaporation of water. Therefore, the left-right heterogeneous structure will increase the water evaporation rate in the small pore size region, so the supersaturation of the solution in the reflow liquid film increases, and the nucleation rate increases sharply, which tends to precipitation to form a cluster structure. As can be seen from Fig. 4(i), the distribution of the precipitated salt is more dispersed throughout the space, and there is no severe blockage of the inlet and outlet channels. Therefore, it can also be seen from the pressure drop results in Fig. 5(b) that the pressure drop gradually decreases after 6 h and eventually

stabilizes at about 1 kPa. Hence, it has little effect on the continuous injection of CO_2.

Fig. S3 (see the attachment) is the salt precipitation process (LR-2) of the left-right heterogeneous micromodel at a CO_2 injection rate of 0.5 mL/min. From Fig. S3(c), it can be seen that the residual solution state is reached after 1.5 h of CO_2 injection, and the residual solution is mainly distributed in the porous area with a small aperture. As CO_2 is continuously injected, the salt precipitates and grows (see Figs. S3(d)-S3(i)), and finally, the solution evaporates completely after 7.4 h (see Fig. S3(i)). From the microscopic results of salt precipitation in Fig. 6(e), it can be seen that the salt precipitated is almost cluster structure. Therefore, increasing the CO_2 injection rate can further increase the supersaturation of the solution, eventually forming a cluster structure. The precipitated salt is dispersed throughout the micromodel, and there is no serious blockage of the inlet and outlet channels. Therefore, it can be seen from the pressure drop results in Fig. 5(b) that the pressure drop gradually decreases and finally stabilizes at about 5 kPa after 1.5 h, which has little effect on the continuous injection of CO_2.

Fig. S4 (see the attachment) is the salt precipitation process (LR-3) of the left-right heterogeneous micromodel at a CO_2 injection rate of 2 mL/min. It can be seen from Fig. S4(c) that the residual solution state is reached after 120 min of CO_2 injection, and the residual solution is distributed in the porous area with large and small pore sizes. As CO_2 is continuously injected, the salt precipitates and grows (as shown in Figs. S4(d)-S4(i)), and finally, the solution evaporates completely after 150 min (as shown in Fig. S4(i)). Compared with the results of the CO_2 injection rate of 0.1 (Fig. 4(i)) and 0.5 mL/min (Fig. S3(i)), it can be found that with the increase of the CO_2 injection rate, the time required for evaporation decreases sharply, indicating that the water evaporation rate increases. From the microscopic results of salt precipitation in Fig. 6(f), it can be seen that the precipitated salts are clustered, because the water evaporation rate growth with the further increase of the CO_2 injection rate. On the one hand, the salt solute cannot diffuse into the residual solution in time. On the other hand, increasing the CO_2 injection rate can further increase the supersaturation of the solution, eventually growing up to form a cluster structure. Therefore, the salt tends to precipitate ectopically at the evaporation front, and the precipitated salt is dispersed throughout the space without seriously blocking the inlet and outlet channels. Therefore, it can be seen from the pressure drop results in Fig. 5(b) that the pressure drop gradually decreases after 120 min and eventually stabilizes at about 18 kPa, which has little effect on the continuous injection of CO_2.

Regardless of the CO_2 injection rate, the salt is precipitated in a cluster-like microstructure in the left-right heterogeneous structures, and the salt is more dispersed in the micromodel. The distribution maintains the flow channel of CO_2, so it has little effect on injectivity. Compared with the results of homogeneous porous media (He et al., 2019), under hydrophilic conditions, when the injection rate of carbon dioxide is small, salt will accumulate locally in the inlet and mainstream area, and the pressure drop will increase sharply to a larger value.

Salt precipitation will seriously damage the injectivity. Therefore, whether it is the up-down or left-right heterogeneous structure, even under a low CO_2 injection rate, it can avoid the local aggregation of salt in the inlet and mainstream area, thus alleviating the influence of salt precipitation on the injectivity.

3.3 Composite micromodel

Fig. 7 is the salt precipitation process (CO-1) at a CO_2 injection rate of 0.1 mL/min in the composite micromodel. The micromodel begins to fill with NaCl solution. With the continuous injection of CO_2, the solution in the large-aperture porous area near the injection inlet begins to be displaced. As shown in Fig. 7(b), CO_2 reaches the fracture. Because the size of the fracture is much larger than the pore throat of the porous medium on both sides, the capillary pressure is small, and CO_2 preferentially passes through and breaks through the fracture. After the breakthrough of CO_2, with the continuous injection of CO_2, the water in the solution continues to evaporate, as shown in Fig. 7(c), and salt precipitation begins near the injection port. Subsequently, at 5 h, as shown in Fig. 7(d), it can be observed that salt precipitation began to appear at the front end of the fracture and gradually occupied the width of the entire fracture channel. Due to the continuous precipitation and accumulation of salt in the fracture, the micro-porous media formed by the precipitated salt are becoming denser and denser, increasing the resistance of CO_2 passing through the fracture, which is ultimately more incredible than the resistance in the porous media with small pore sizes on both sides. After 9.7 h of CO_2 injection (as shown in Fig. 7(e)), CO_2 flows selectively in the porous media on both sides of the fracture and forms a breakthrough path. After 48 h of CO_2 injection (as shown in Fig. 7(g)), due to the continuous injection of CO_2 in the newly formed path, the porous media on both sides of the fracture are continuously precipitated with salt in the pore throat, resulting in blockage. Therefore, CO_2 begins to displace the remaining residual solution and form more breakthrough channels, as shown in the blue arrow in Fig. 7(g). Due to the blockage of the precipitated salt to the fracture, the injection rate of CO_2 in the fracture is low. Therefore, most of the CO_2 is re-selected to pass through new channels in the porous media on both sides of the fracture, the residual solution is continuously evaporated, and salt is constantly precipitated in the porous media, while there is almost no new salt precipitation in the fracture. As shown in Fig. 7(i), the solution is completely evaporated.

Fig. 8 is the microscopic result of the complete evaporation of the residual solution. From Figs. 8(b) and 8(c), it can be seen that the front end of the fracture is filled with precipitated salt. The structure of precipitated salt in the fracture is mainly the crystal structure and cluster structure with apparent edges and corners. The crystal structure of the salt has no finer hollow channels, so CO_2 can't pass through, resulting in a complete blockage of the fracture, which also explains the formation of the new CO_2 path in Fig. 7. In the porous media on both sides of the fracture (as shown in the purple box marker in the figure), the salt precipitation is mostly a colorless and transparent crystal structure. As shown in Fig. 8(d), the
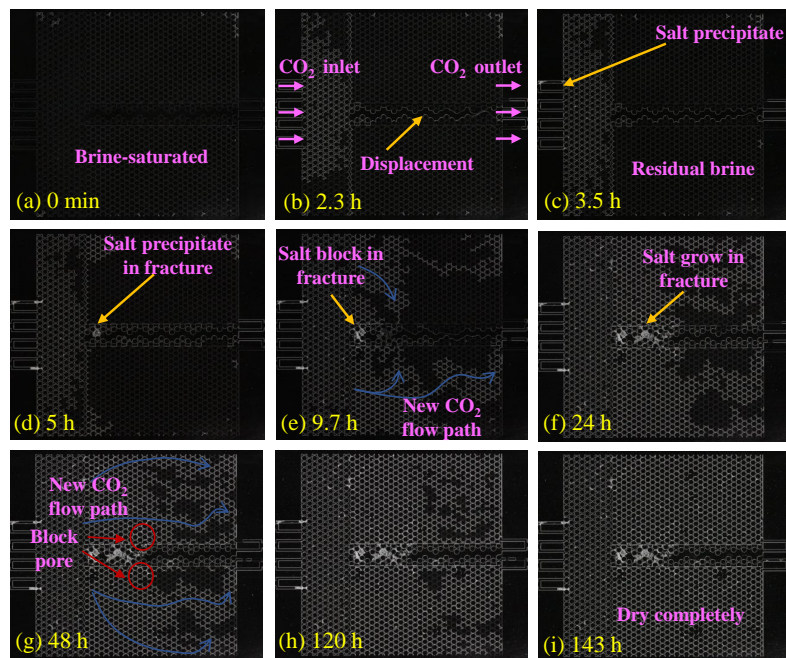
Fig. 7. Salt precipitation process of case CO-1.
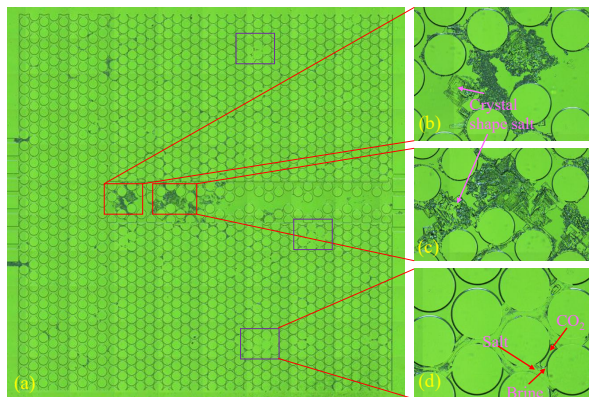
Fig. 8. Microscopic results of salt precipitation of composite micromodel with a CO_2 injection rate of 0.1 mL/min.

crystal structure formed by the precipitated salt occupies the pore space of the porous medium. A unique phenomenon is also found in the figure, inside the crystal of the precipitated salt, a hole appears, with the residual solution and CO_2 gas inside, which is trapped by the solid wall structure and the precipitated crystal, thus wholly isolated from the outside environment and forming a stable state. This phenomenon is similar to inclusions in geology (Shepherd et al., 1985; Liu et al., 2011), so the discovery is instructive for the formation process and manner of inclusions. Fig. 9(a) is the pressure drop result of the salt precipitation process. It can be seen from the figure that the pressure drop curve has multiple pulsations, which are caused by the multiple blockages of the fractures and the formation of new channels. Although the precipitated salt blocks the front fracture after the solution is completely evaporated, a large number of CO_2 channels are formed in the small-aperture porous areas on both sides of the fracture, and

the final pressure drop is reduced to a lower value, which has little effect on CO_2 injection.

Fig. S5 (see the attachment) is the salt precipitation process (CO-2) when the CO_2 injection rate increases to 2 mL/min. It can be seen from Fig. S5(b) that when the displacement reaches 16 min, at a lower injection rate, CO_2 has preferentially broken through the fracture. Due to the continuous water evaporation, salt precipitation began near the injection port at 1.1 h (Fig.S5 (c)). With the continuous injection of CO_2, the pressure difference between the inlet and outlet gradually accumulates and increases. When the pressure difference increases enough to break through the capillary pressure of the small aperture porous medium on both sides of the fracture, the solution in the porous medium begins to be displaced. Thereafter, as shown in Figs. S5(c)-S5(e), salt continues to grow and spread. It can be observed from Fig. S5(f) that at the back end of the fracture, the precipitated salt has completely occupied the width of the fracture. Because there are more residual solutions in the pores around the fracture so that the salt here can continue to grow and eventually occupy the entire fracture. In addition, since CO_2 can enter the porous media on both sides of the fracture, the water in the residual solution is continuously evaporated. Finally the solution is completely evaporated after 8 h (Fig. S5(i)). Fig. 10 is the microscopic result diagram after complete evaporation. It can be seen from the diagram that the amount of salt precipitation in the fracture is less, and the salt is cluster structure. Because when the injection rate of CO_2 increases, a large number of solutions in the porous medium will be displaced so that the amount of residual solution is less. It can also be seen from the diagram that there are fewer residual solutions on both sides of the fracture. Therefore, there is no sufficient solution when salt precipitation occurs in the fracture so that the salt cannot be
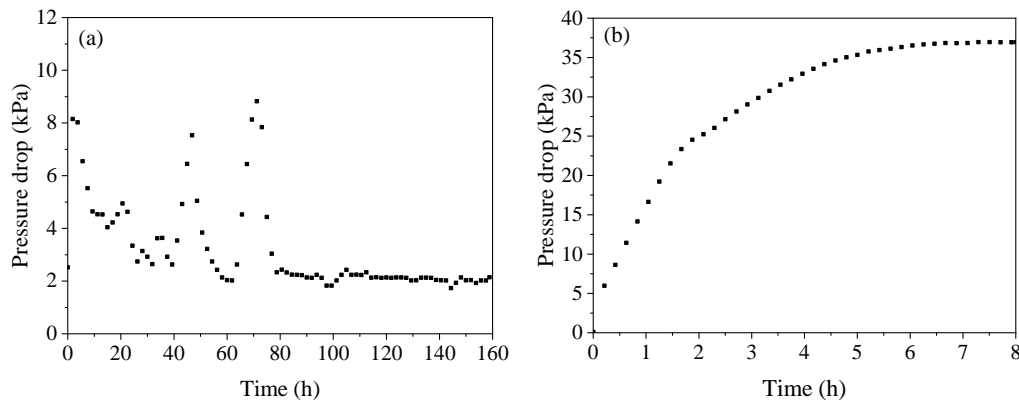
Fig. 9. Pressure drop results of composite micromodel: (a) case CO-1 and (b) case CO-2.
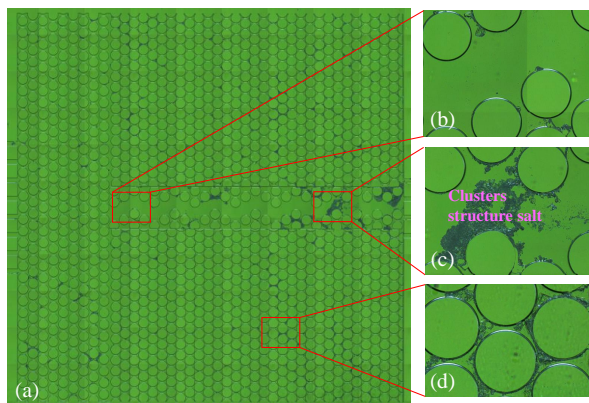
Fig. 10. Salt precipitation microscopic results of CO_2 injection rate of 2 mL/min in composite micromodel.

fully grown in the fracture, and there is no phenomenon that the salt fills the entire fracture width. The pressure drop results are shown in Fig. 9(b). It can be seen from the figure that the pressure drop gradually increases to 36 kPa, and there is no pressure pulsation. Because the salt precipitated in the early stage does not completely block the fracture. The accumulated pressure first breaks through the solution on both sides of the fracture, so the pressure monotonically increases and stabilizes at 36 kPa. The precipitated salt has little effect on the continuous injection of CO_2.

4. Conclusion

The salt precipitation behavior in different structures (up-down heterogeneous, left-right heterogeneous, and composite structure) was studied by pore-scale experiments. Whether the up-down or left-right heterogeneous structure, even under a low CO_2 injection rate, can avoid the local aggregation of salt in the inlet and mainstream area, thus alleviating the influence of salt precipitation on the injectivity. When the CO_2 injection rate is low in the composite structure, the salt is mainly precipitated in the fracture and porous area as a crystal structure, which blocks the fracture.

In summary, the injection well can be selected in the formation with strong heterogeneity to alleviate the blockage caused by salt precipitation. While it's important to note that

the heterogeneity of the reservoir promotes the formation of dominant channels, leading to faster breakthroughs and reduced displacement efficiency for CO_2-EOR and storage capacity for CO_2 storage. Therefore, it is recommended to select heterogeneous formations near injection wells, while homogeneous reservoirs are preferred in most areas away from injection wells. When CO_2 leaks in the caprock fractures, salt is easy to grow in the fractures until the fractures are blocked. This phenomenon is of great significance to the salt precipitation self-healing of caprock fractures.

Supplementary file

https://doi.org/10.46690/ager.2023.03.05

Conflict of interest

The authors declare no competing interest.

References

Akindipe, D., Saraji, S., Piri, M. Salt precipitation during geological sequestration of supercritical CO_2 in saline aquifers: A pore-scale experimental investigation. Advances in Water Resources, 2021, 155: 104011.

Bacci, G., Durucan, S., Korre, A. Experimental and numerical study of the effects of halite scaling on injectivity and seal performance during CO_2 injection in saline aquifers.

Energy Procedia, 2013, 37: 3275-3282.

Bacci, G., Korre, A., Durucan, S. Experimental investigation into salt precipitation during CO_2 injection in saline aquifers. Energy Procedia, 2011, 4: 4450-4456.

Baumann, G., Henninges, J., De Lucia, M. Monitoring of saturation changes and salt precipitation during CO_2 injection using pulsed neutron-gamma logging at the ketzin pilot site. International Journal of Greenhouse Gas Control, 2014, 28: 134-146.

Bentham, M., Kirby, M. CO_2 storage in saline aquifers. Oil and Gas Science and Technology, 2005, 60(3): 559-567.

Bergstad, M., Or, D., Withers, P. J., et al. Retracted: Evaporation dynamics and NaCl precipitation on capillarity-coupled heterogeneous porous surfaces. Water Resources Research, 2018, 54(6): 3876-3885.

Cai, J., Chen, Y., Liu, Y., et al. Capillary imbibition and flow of wetting liquid in irregular capillaries: A 100-year review. Advances in Colloid and Interface Science, 2022, 304: 102654.

Cai, J., Perfect, E., Cheng, C., et al. Generalized modeling of spontaneous imbibition based on hagen-poiseuille flow in tortuous capillaries with variably shaped apertures. Langmuir, 2014, 30(18): 5142-5151.

Cui, G., Hu, Z., Ning, F., et al. A review of salt precipitation during CO_2 injection into saline aquifers and its potential impact on carbon sequestration projects in China. Fuel, 2023, 334: 126615.

De Yoreo, J. J., Vekilov, P. G. Principles of crystal nucleation and growth. Reviews in Mineralogy and Geochemistry, 2003, 54(1): 57-93.

Duong, C., Bower, C., Hume, K., et al. Quest carbon capture and storage offset project: Findings and learnings from 1st reporting period. International Journal of Greenhouse Gas Control, 2019, 89: 65-75.

Grude, S., Landrø, M., Dvorkin, J. Pressure effects caused by CO_2 injection in the Tubåen Fm., the Snøhvit field. International Journal of Greenhouse Gas Control, 2014, 27: 178-187.

He, D., Jiang, P., Xu, R. Pore-scale experimental investigation of the supercritical CO_2 injection rate and the surface wettability on salt precipitation. Environmental Science and Technology, 2019, 53(24): 14744-14751.

He, D., Xu, R., Ji, T., et al. Experimental investigation of the mechanism of salt precipitation in the fracture during CO_2 geological sequestration. International Journal of Greenhouse Gas Control, 2022, 118: 103693.

Hu, X., Wang, J., Zhang, L., et al. Direct visualization of nanoscale salt precipitation and dissolution dynamics during CO_2 injection. Energies, 2022, 15(24): 9567.

Kim, M., Sell, A., Sinton, D. Aquifer-on-a-chip: Understanding pore-scale salt precipitation dynamics during CO_2 sequestration. Lab on a Chip, 2013, 13(13): 2508-2518.

Li, R., Jiang, P., Gao, C., et al. Experimental investigation of silica-based nanofluid enhanced oil recovery: The effect of wettability alteration. Energy & Fuels, 2017, 31(1): 188-197.

Liu, N., Liu, L., Qu, X., et al. Genesis of authigene carbonate minerals in the upper cretaceous reservoir, honggang anticline, songliao basin: A natural analog for mineral trapping of natural CO_2 storage. Sedimentary Geology, 2011, 237(3-4): 166-178.

Liu, H., Zhu, Z., Patrick, W., et al. Pore-scale numerical simulation of supercritical CO_2 migration in porous and fractured media saturated with water. Advances in Geo-Energy Research, 2020, 4(4): 419-434.

Nooraiepour, M., Fazeli, H., Miri, R., et al. Effect of CO_2 phase states and flow rate on salt precipitation in shale caprocks-a microfluidic study. Environmental Science and Technology, 2018, 52(10): 6050-6060.

Norouzi, A. M., Niasar, V., Gluyas, J. G., et al. Analytical solution for predicting salt precipitation during CO_2 injection into saline aquifers in presence of capillary pressure. Water Resources Research, 2022, 58(6): 032612.

Ott, H., Roels, S. M., De Kloe, K. Salt precipitation due to supercritical gas injection: I. Capillary-driven flow in unimodal sandstone. International Journal of Greenhouse Gas Control, 2015, 43: 247-255.

Piao, J., Han, W. S., Choung, S., et al. Dynamic behavior of CO_2 in a wellbore and storage formation: Wellbore-coupled and salt-precipitation processes during geologic CO_2 sequestration. Geofluids, 2018, 2018: 1789278.

Ren, J., Wang, Y., Feng, D., et al. CO_2 migration and distribution in multiscale-heterogeneous deep saline aquifers. Advances in Geo-Energy Research, 2021, 5(3): 333-346.

Salih, H. H., Li, J., Kaplan, R., et al. Life cycle assessment of treatment and handling options for a highly saline brine extracted from a potential CO_2 storage site. Water Research, 2017, 122: 419-430.

Shepherd, T. J., Rankin, A. H., Alderton, D. H. M. A Practical Guide to Fluid Inclusion Studies. New York, USA, Blackie Chapman and Hall, 1985.

Tang, Y., Yang, R., Du, Z., et al. Experimental study of formation damage caused by complete water vaporization and salt precipitation in sandstone reservoirs. Transport in Porous Media, 2015, 107: 205-218.

Vialle, S., Druhan, J. L., Maher, K. Multi-phase flow simulation of CO_2 leakage through a fractured caprock in response to mitigation strategies. International Journal of Greenhouse Gas Control, 2016, 44: 11-25.

Wang, Y., Luce, T., Ishizawa, C., et al. Halite precipitation and permeability assessment during supercritical CO_2 core flood. Paper SCA2010-18 Presented at International Symposium of the Society of Core Analysts, Halifax, Nova Scotia, Canada, 4-7 October, 2010.

Wang, Y., Mackie, E., Rohan, J., et al. Experimental study on halite precipitation during CO_2 sequestration. Paper SCA2009-25 Presented at International Symposium of the Society of Core Analysts, Noordwijk, The Netherlands, 27-30 September, 2009.

Xu, R., Li, R., Huang, F., et al. Pore-scale visualization on a depressurization-induced CO_2 exsolution. Science Bulletin, 2017, 62(11): 795-803.

Yang, F., Bai, B., Dunn-Norman, S., et al. Factors affecting CO_2 storage capacity and efficiency with water withdrawal in shallow saline aquifers. Environmental Earth Sciences, 2014, 71: 267-275.